MM309 PROJECT
APPLICATIONS OF MOLECULAR DYNAMICS IN MATERIALS SCIENCE ENGINEERING

GROUP 3
Members:
Aditya Handa(200005004)
Akshita Mittal(200005005)
Anirudh Bhagwat(200005006)
Daksh Goyal(200005012)
Sejal Kotian(200005042)

Introduction to Molecular Dynamics

Molecular dynamics (MD) is a computer simulation method for analyzing the physical movements of atoms and molecules. For a fixed amount of time, the atoms and molecules are allowed to interact, providing insight into the system's dynamic "evolution.". Most commonly, Newton's Equations of Motion for a system of interacting particles are numerically solved to determine the trajectories of atoms and molecules. To calculate the forces between the particles and their potential energies, interatomic potentials or molecular mechanics force fields are frequently used. This approach is mainly used in the fields of biophysics, materials science, physics, and chemistry.

MD method does not require the model simplified too much, and researchers can directly sum to realize the estimation of statistics in macroscopic phenomenon based on the molecular (atoms, ion) arrangements and the simulated results of the movements. It can directly simulate many macroscopic phenomena and obtain consistent or comparable results with experiments. It can also provide microscopic structure, and movements

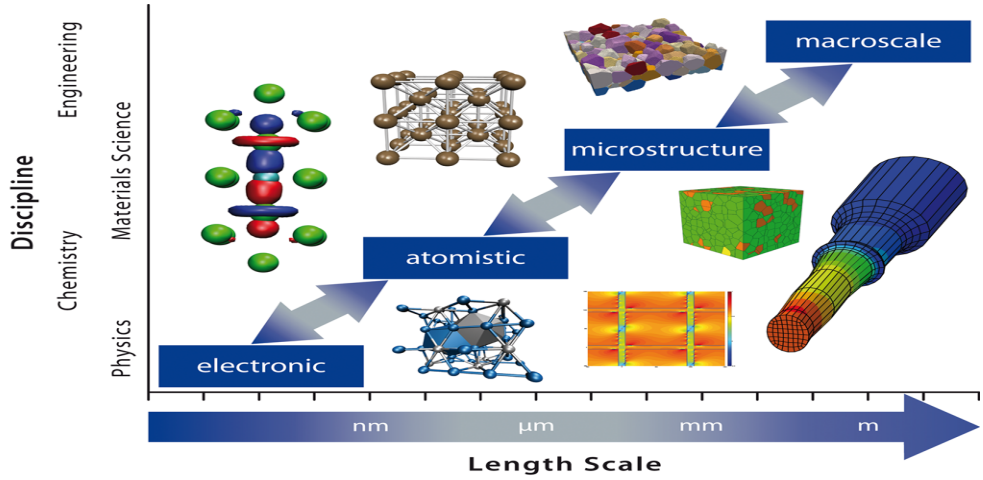

Molecular dynamics simulation

The basic principle of simulation:
Molecular dynamics simulation is a simulated computer method, through the equations for a group of interactive atomic motion equations, investigates its evolutionary behavior over time. In a molecular dynamics simulation, the movement of atoms follows the classical mechanics required by Newton's laws. In a system formed by N atoms, with other atoms interacting with each other, the force received by each atom as

$$m_j \frac{d^2\mathbf{r}_j}{dt^2} = \mathbf{F}_j, \qquad \mathbf{F}_j = -\frac{\partial V}{\partial \mathbf{r}_j}, \qquad j = 1,2,\cdots,N$$

The above equation shows that molecular dynamics is a deterministic method, that is, given an initial position and initial velocity, the whole system along with the time evolution locus can be completely determined theoretically.

Molecular dynamics numerical method:
The molecular dynamics numerical method is based on the familiar Newton motion equation. Given an initial speed and displacement to the atoms whose quality is m, the force every atom which is embedded in the atomic method (EAM) received could be calculated. Then a new speed and displacement will be obtained based on a dynamic equation. In the actual numerical calculation, dt can't be too small, or the complete simulation is likely to spend too much time. Molecular dynamics involves different algorithms, commonly used as the following:

1)Verlet Algorithm

$$x_i(t+\Delta t) = x_i(t) + v_i(t)(\Delta t) + \frac{1}{2!}a_i(t)(\Delta t)^2$$

$$v_i(t+\Delta t) = v_i(t) + \frac{\Delta t}{2}\left(\frac{F(t)+F(t+\Delta t)}{m}\right)$$

General Procedure:
1)Find the position
2)Find Force
3)Find the Velocity and repeat

This will generate trajectories of position and velocity computed at t=0; t=delta t, t= 2*delta t, t=3*delta and so on.

2)Gear Algorithm

Predictor stage

$$\vec{r}_i^{\,p}(t+\delta t) = \vec{r}_i(t) + \vec{v}_i(t)\delta t + \frac{1}{2}\vec{a}_i(t)\delta t^2 + \frac{1}{6}\vec{b}_i(t)\delta t^3$$

$$\vec{v}_i^{\,p}(t+\delta t) = \vec{v}_i(t) + \vec{a}_i(t)\delta t + \frac{1}{2}\vec{b}_i(t)\delta t^2$$

$$\vec{a}_i^{\,p}(t+\delta t) = \vec{a}_i(t) + \vec{b}_i(t)\delta t$$

$$\vec{b}_i^{\,p}(t+\delta t) = \vec{b}_i(t)$$

The gear predictor-corrector algorithm predicts the next set of positions and accelerations and then compares the accelerations and predictions to commute a correction for each step. Each step is thus refined literately.

The predictor uses Taylor Series up to higher order(qth order) derivatives at each time step. Coefficients are tabulated for the qth-order predictor.

Applications of Molecular Dynamics in Materials Science Engineering

1)Applications in the Nanocrystalline Cutting process.
2)Applications in Carbon Nanotubes
3)Application in the Solidification and Melting
4)Application in the Mechanical Deformation of Nanocrystalline materials
5)Applications in Nanoindentation Measurement

Research Article Summary
Research Article 1

MOLECULAR DYNAMICS SIMULATION OF THE NANOMETRIC CUTTING PROCESS

Q. X. PEI* and C. LU Institute of High Performance Computing 1 Science Park Road, Singapore 117528
F. Z. FANG and H. WU Singapore Institute of Manufacturing Technology 71 Nanyang Drive, Singapore 638075

-Aditya Handa

Abstract

Nanoscale machining involves changes in only a few atomic layers at the surface. Molecular dynamics (MD) simulation can play a significant role in addressing a number of machining problems at the atomic scale. This paper implements MD simulations to study the nanometric cutting process of single-crystal copper. Instead of the widely used Morse potential, we used the Embedded Atom Method (EAM) potential for this study. The simulations were carried out for various tool geometries at different cutting speeds. Attention was paid to the cutting chip formation, the cutting surface morphology, and the cutting force. The MD simulation results show that both the tool geometry and the cutting speed have a great influence on the chip formation, the smoothness of the machined surface, and the cutting force.

Introduction

Nanoscale machining involves changes in only a few atomic layers at the surface. Molecular dynamics (MD) simulation can play a significant role in addressing a number of machining problems at the atomic scale.

Nanometric machining is a tool-based material removal process that generates ultraprecision surfaces at a nanometer scale. With the advance of science and

technology, there is an increasing demand for the manufacture of miniaturized components in the field of aviation, aerospace, medical instruments, etc.

However, as nanometric machining involves changes in only a few atomic layers at the surface, it is extremely difficult to observe the machining process and to measure the process parameters through experiments. So, molecular dynamics (MD) simulation has become an important tool to study the nanometric machining process.

Simulation Model

The workpiece consists of 10500 atoms with the dimensions of 35a × 15a × 5a, where a is the lattice constant of copper (3.62 Å). As copper is much softer than diamond, it is a good approximation to take the tool as a rigid body. Three different tool geometries with the rake angle α of 45°, 0°, and –45° are used in the study. The tool clearance angle β is 10°. The cutting speeds used ranged from 10.0 to 100.0 m/s with the depth of cut being 1.08 nm.

The boundary conditions of the nano-machining simulation include: (1) The two layers of the atoms in the y–z faces (left side of the work material) and the lower x–z plane (bottom of the work material) are kept fixed. (2) Periodic boundary conditions are maintained along the z direction. The EAM potential was used for the copper workpiece to consider the many-body effect due to metallic bonding.

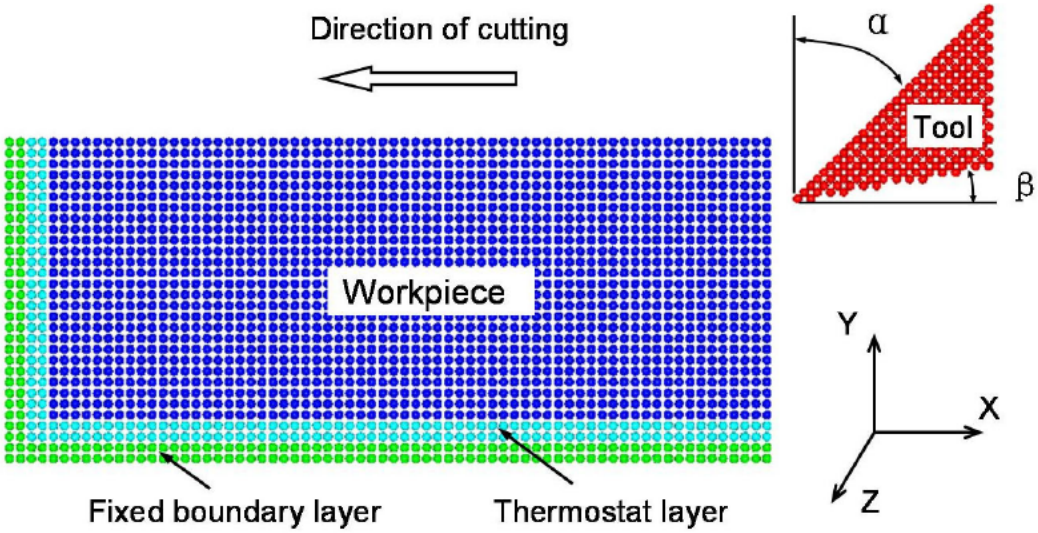

Simulation Results and Discussion

The simulated nanoscale cutting processes at the cutting speed of 100 m/s for the different tool angles are shown. Different geometry of cutting tools results in different atomic distortions in tools' affinity and abrasive actions.

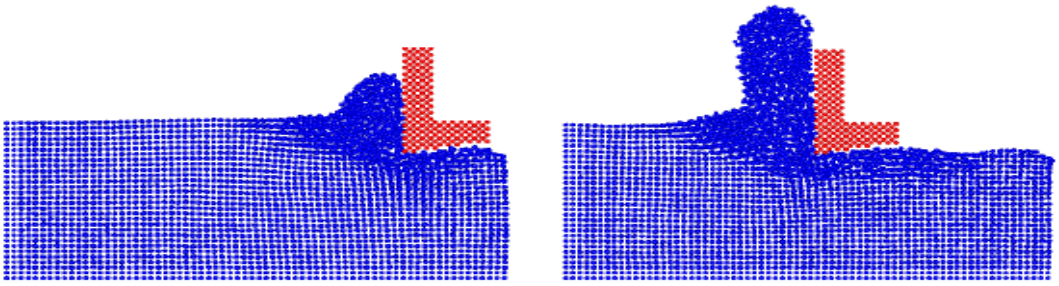

(a) Time = 35 ps (b) Time = 70 ps

Fig. 2. The nanometric cutting process with the tool rake angle 0° and the cutting speed of 100 m/s.

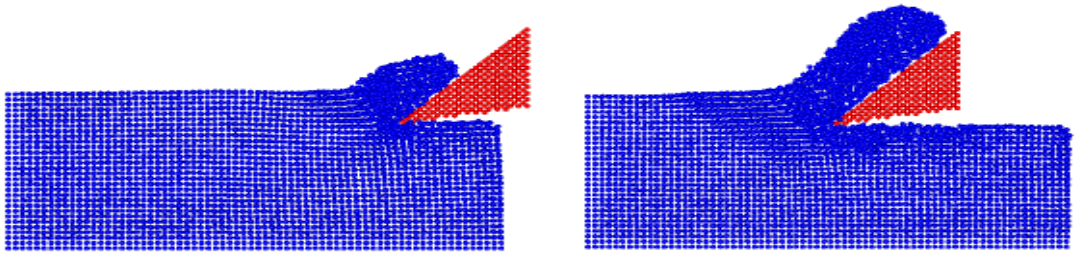

(a) Time = 35 ps (b) Time = 70 ps

Fig. 3. The nanometric cutting process with the tool rake angle 45° and the cutting speed of 100 m/s.

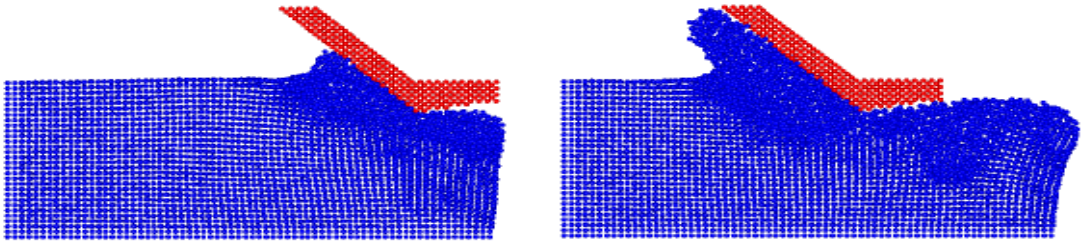

(a) Time = 35 ps (b) Time = 70 ps

Fig. 4. The nanometric cutting process with the tool rake angle –45° and the cutting speed of 100 m/s.

From the simulation results with the rake angle of 45° (Fig. 3), it can be seen that although the basic cutting process is similar to that with the 0° rake angle analyzed above, there are also some obvious differences resulting from the different rake angles. As the tool's 45° rake angle is very sharp, the chip mainly undergoes shear deformation and moves along the tool surface in the 45° direction. The machined surface is smoother than that with a 0° rake angle.

At this lower cutting speed, it can be seen that the chips are shorter and thicker than that with the higher cutting speed

Conclusions

MD simulations of copper nanoscale cutting processes were carried out with EAM potential for different tool rake angles and different cutting speeds. The simulation results show that:

• The tool rake angle has a big effect on the material removal and chip formation. As the rake angle decreases from 45° to –45°, the chip deforms from more shear deformation to more compression deformation, and the machined surface becomes rougher.

• As the rake angle decreases from 45° to –45°, both the horizontal and vertical cutting forces increase significantly. Therefore, a much bigger cutting force is needed for the tool with the rake angle –45° than that with the rake angle of 45°.

• The cutting speed has an obvious effect on the chip formation and machined surface. The low cutting speed favors a smooth surface, while the high cutting speed results in a rough surface.

References

1. Z. C. Lin and J. C. Huang, Nanotechnology 15, 510 (2004).
2. Y. Y. Ye, R. Biswas, J. R. Morris, A. Bastawros and A. Chandra, Nanotechnology 14, 390 (2003).
3. T. H. Fang and C. I. Weng, Nanotechnology 11, 148 (2000).
4. R. Komanduri, N. Chandrasekaran and L. M. Raff, Wear 242, 60 (2000).
5. L. Zhang and H. Tanaka, Wear 211, 45 (1997).
6. K. Maekawa and A. Itoh, Wear 188, 115 (1995). Int. J. Nanosci.
7. S. Shimada, N. Ikawa, H. Tanaka and J. Uchikoshi, Ann. CIRP 43, 51 (1994).
8. I. Inamura, and N. Takezawa, Ann. CIRP 41, 121 (1992).
9. M. S. Dow, S. M. Foiles and M. I. Baskes, Mater. Sci. Rep. 9, 251 (1993).
10. M. S. Dow and M. I. Baskes, Phys. Rev. B 29, 6443 (1984).

Research Article 2

Molecular dynamics simulations of the elastic properties of polymer/carbon nanotube composites

-Akshita Mittal

CNT's are promising additives to Polymeric Materials
Potential for enhancement of mechanical, chemical and electronic properties
Improvements are not guaranteed, and results depend on the polymer chosen, quantity and quality of the CNT

In this paper, Classical molecular dynamics (MD) simulations of model polymer/CNT composites are done:
constructed by embedding a **single wall (10,10) CNT** into two different amorphous polymer matrices:

- poly(methyl methacrylate) **(PMMA)**
- poly{(m-phenylene- vinylene)-co-[(2,5-dioctoxy-p-phenylene) vinylene]} **(PmPV)**
  with **different volume fractions**

A constant-strain energy minimization method was then applied to calculate the **axial and transverse elastic moduli** of the composite system.

Building Polymer Model

Two chains of PMMA (80% syndiotactic), each with 50 repeat units, were built in a periodic box with initial density of 0.1 g cm3 using the **DREIDING force field parameters.**

The model was put into an **NPT ensemble simulation**
pressure = 10 atm
temperature = 500 K for 1 ns (the simulation time step was 1 fs).

The purpose of this step was to slowly compress the structure to generate initial amorphous matrix with the correct density and low resid- ual stresses. Attempts

to further increase pressure using the **DREIDING force field** failed to generate a density close to the experimental value.

The COMPASS force field was then applied under the same conditions for another 500 ps. The simulation temperature was then set to 298 K, and pressure of 1 atm for another 500 ps. The density of the final matrix was 1.15 g/cm3, which is very close to the experimental value of 1.19 g/cm3

After this, a constant-strain minimization was carried out with the strain being varied from 0% to 2% in discrete steps

Computational results
A (10,10) SWNT was placed in the centre of a periodic simulation cell. PmPV molecules with different number of repeat units were then placed randomly around the tube in non-overlapping positions.

A similar equilibration process as used for generating the matrix model was then applied to generate the composite model.

Research Article 3

APPLICATION OF MD IN STUDYING SOLIDIFICATION AND REMELTING PROCESSES OF ALUMINIUM

-Anirudha Bhagwat

Abstract

Sutton-Chen many body potential has been used in a molecular dynamics simulation study to look into the solidification and remelting of aluminum. To discover the right size for the system, various atom counts between 108 and 2048 were taken into consideration. The radial distribution function was used to assess the system's structural makeup. By computing the variation in heat capacity throughout the phase transformation, the melting and crystallization temperatures of aluminum were assessed. The glass transition temperature was also determined using Wendt-Abraham parameters. It has been demonstrated that as the heating rate rises, aluminum's melting temperature rises as well. Depending on the conditions, a crystalline or amorphous-looking structure develops during solidification.

Introduction

During the rapid solidification of metals, amorphous and crystalline structures can be formed depending on the cooling rate. At high cooling rates, the crystallization may be suppressed and a metastable amorphous structure (metallic glass) is formed. Under such circumstances, the liquid structure with a short-range order is saved in the solid (amorphous) state.

The study of the crystallization and glass formation processes of metals during rapid solidification has made extensive use of the highly effective technique known as molecular dynamics simulation.The MD simulation results offer insight into the local structural features and the accompanying thermal dynamics qualities under strong quenching settings since the cooling rates employed in MD simulations are typically higher than the laboratory quick quenching investigations.

Literature Review

Simulations

An ISO/ANSI C++ standard code was developed to run equilibrium MD simulation in the canonical ensemble (NVT) with a constant number of atoms (N), volume (V) and temperature (T) with a time step of 0.1 fs. The periodic boundary conditions (PBC) were applied on the three dimensions of the MD cell. The equations of motion of the system were numerically solved using the velocity version of the Verlet algorithm with an integration step size of 10 fs.

The energy is given as

In order to choose an adequate number of atoms, different systems with different numbers of atoms, i.e. 108, 256, 500, 864, 1372 and 2048, were considered for the melting process. These numbers of atoms were considered because of the simulation cell shape (cube) and the atomic structure of solid aluminum, which is fcc, in order to fill the whole cell. The simulation run was applied for 25 ps at 300 K for equilibration. Then, the temperature was gradually increased from 300 K to 1300 K with a heating rate of 10^12 K/s.

In order to study melting, solidification and the remelting processes of aluminum, 500 atoms were considered. To attain equilibrium, the simulation run was applied for 25 ps at 300 K. The temperature was then gradually increased from 300 K to 1300 K at three different rates of 1012, 1013 and 1014 K/s. At 1300 K the system was maintained for 5 ps and subsequently was cooled to 300 K at the same rate it was heated. After another relaxation time at 300 K for 5 ps, the temperature gradually increased up to 1300 K at the mentioned heating rates.

Summary

No. of atoms	Melting temperature (K)
108	1060
256	970
500	940
864	940
1372	940
2048	940

From the sudden changes in internal energy of systems which are related to the melting of the systems, the melting points are calculated. As can be seen, the melting point lowered from 1060 K for 108 atoms to 940 K for 500 atoms. The melting point did not change for larger systems. Therefore, 500 atoms were considered for the next simulation. The reason for this temperature drop is based on the stability of the system; the system needs a minimum number of atoms to be stable.
Figure 2 shows the internal energy of the system as a function of temperature during heating of the system from 300 K to 1300 K. At the heating rate of 10^12 K/s, a sudden increase in the internal energy in the temperature range of 896-907 K occurred.

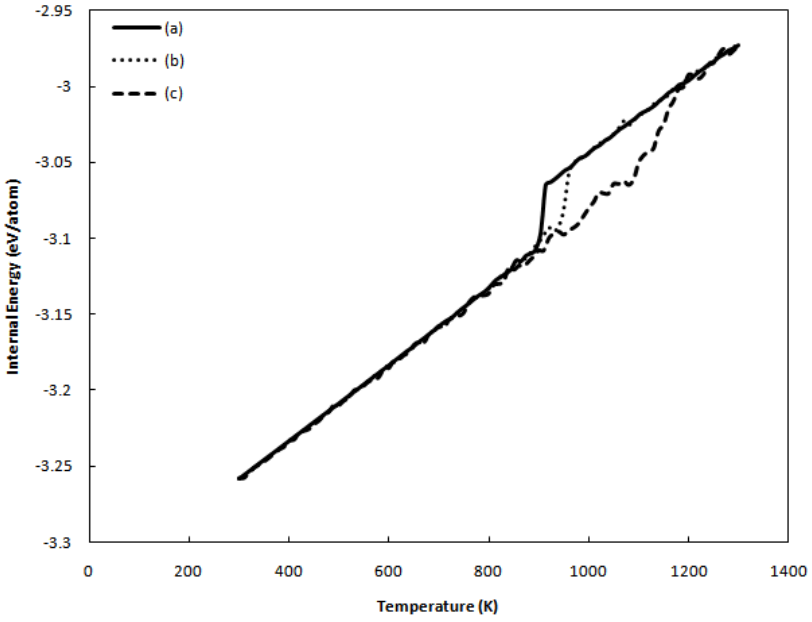

Figure 4 shows the internal energy of the system during the cooling process of the melted aluminum as a function of temperature depending on the freezing rate. Based on the variation of the internal energy. It appears that crystallization of the melt occurred at the cooling rate of 1012 K/s. The crystallization temperature was around 460 K.

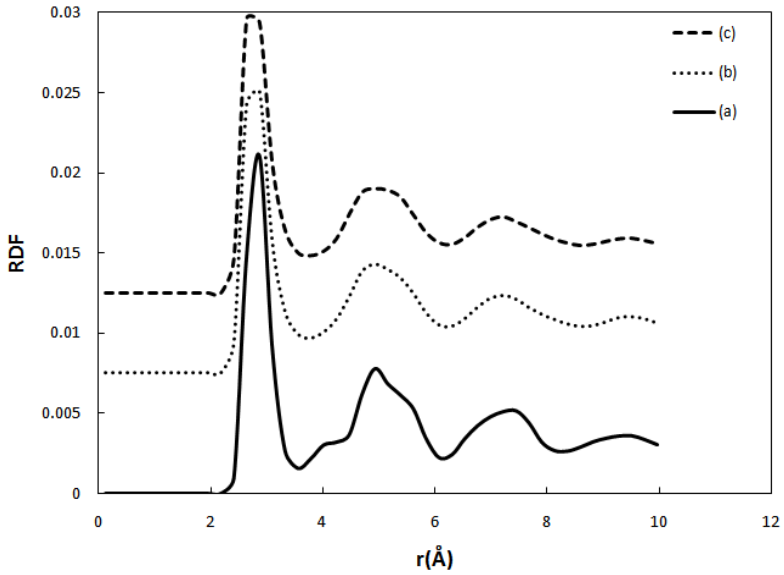

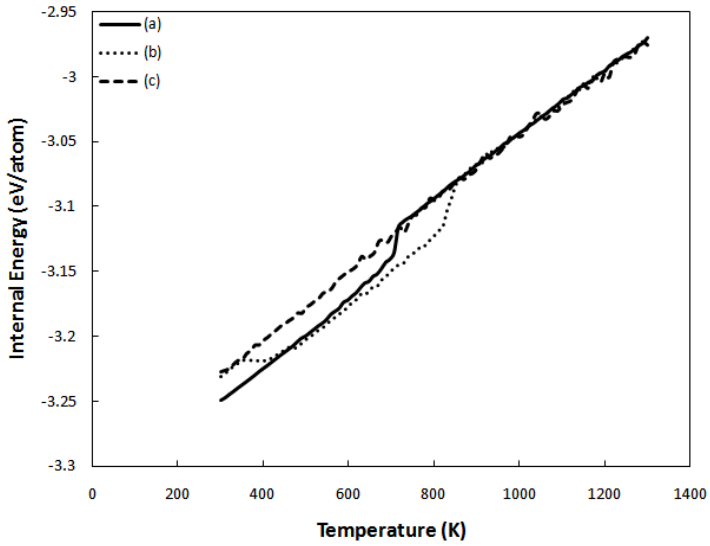

References:-

https://www.researchgate.net/publication/260337336

Research Article 4

Molecular - Dynamics Study of Mechanical Deformation in Nano-Crystalline Aluminum

- Daksh Goyal

Abstract:

INTRODUCTION

NANO-CRYSTALLINE metals exhibit physical properties different from ordinary poly-crystalline materials, which make these materials of technological interest. One important example is the increasing hardness with decreasing grain size, attributed to dislocation immobilization at the grain boundaries, and known as the “Hall–Petch effect. However, for grain sizes below a critical value, the hardness decreases with decreasing grain size, i.e., an inverse Hall– Petch effect. There is still a debate whether this effect is an artifact due to difficulties in sample preparation at the smallest grain sizes. Atomistic simulations identifying an inverse Hall–Petch relation for Cu, Ni, and for small grain sizes (d 10 nm, where d average grain size) exhibit plasticity dominated by intergrain activities, such as rotation, sliding, and growth.

ABSTRACT

This report on molecular-dynamics (MD) simulations of tensile loading of nano-crystalline Al modeled by an embedded-atom method (EAM) potential. Usage of two different sample preparation methods of the nano-crystalline material allows us to compare mechanical properties for different sample qualities. A Voronoi-constructed polycrystal exhibits nearly no pores and has different mechanical properties compared to a material that is sintered under pressure and temperature from spherical nanoparticles, resulting in a lower-density sample. We found an inverse Hall–Petch relation for the flow stress for grain sizes smaller than 10 nm. Intergranular fracture was observed for the larger Al grain sizes, but not for nano-crystalline Cu.

Computational Methods

We used two different methods to prepare the monocrystalline initial sample configuration. Periodic boundaries were employed in both cases. The first method is a Voronoi construction,where grain centers and orientations are randomly chosen, and a subsequent space filling, with the local orientation determined by the closest grain centre. After annealing at 600 K for 22.5 ps and then equilibrating at 300 K for 22.5 ps, this method gives poly-crystalline structures with polytope grains (Figure 1). The We

report on molecular-dynamics (MD) simulations of tensile loading of nano-crystalline Al modeled by an embedded-atom method (EAM) potential. Usage of two different sample preparation methods of the nano-crystalline material allows us to compare mechanical properties for different sample qualities. A Voronoi-constructed polycrystal exhibits nearly no pores and has different mechanical properties compared to a material that is sintered under pressure and temperature from spherical nanoparticles, resulting in a lower-density sample. We found an inverse Hall–Petch relation for the flow stress for grain sizes smaller than 10 nm. Intergranular fracture was observed for the larger Al grain sizes, but not for nano-crystalline Cu.resulting density is close to ideal (Table I) and the grain boundary thickness is independent of grain size (Figure 2). The latter suggests that the grain boundary structure is independent of grain size, even down to the nanometre regime, which is observed by experimental X-ray absorption fine structure techniques and by previous MD studies. The second method (Figure 3) is to sinter the sample from spherical nanoparticles with different diameters. As the initial configuration, we took a close-packed arrangement obtained by contact-dynamics simulations consisting of 32 nanoparticles with three different diameters having a ratio of 2:3:4. Filling those nanoparticles with a crystal of random orientation and sintering under a pressure of 1 to 2 GPa at a temperature of 600 K for 157.5 ps, followed by a relaxation at zero pressure and T 300 K for 45 ps, results in samples of different density depending on the sinter pressure and the size of the nanoparticles (Table I). The preparation processes (annealing, equilibrating, and sintering) were simulated by rescaling uniformly the coordinates and edge lengths in all directions (x, y, z). The subsequent tensile loading was simulated by rescaling all coordinates and the edge length in the direction to be pulled (z) and relaxing the two other directions (x and y) using a scheme similar to that in Reference 6. The integration time step was varied from 1.5 to 4.5 fs. It should be pointed out that with today’s computational power, deformation rates achievable in MD simulations (

---

107 /s) are orders of magnitude larger than conventional experimental ones. However, it has been shown that in the case of quasi-static yielding at zero temperature, the damage occurring in the material and the deformation mechanisms are basically the same, as compared to nonzero strain rate simulations at ambient temperatures. It has also been pointed out that in spite of these extremely high strain rates, the Coble-creep equation describing grain boundary diffusion in coarse-grained materials can still be reproduced.

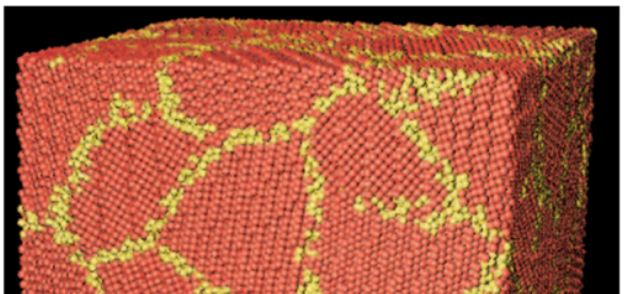

Results

Voronoi-Constructed Samples The tensile loading simulations (Figure 4) show the flow stress decreasing with decreasing grain size, i.e., an inverse Hall–Petch behaviour. The larger the strain rate, the larger the flow stress, which indicates that the material needs a finite response time to activate plasticity (Figure 4). Another interesting observation is the sudden drop in the flow stress for larger grain sizes, which indicates that fracture has occurred. An analysis of the atomic positions indeed shows that intergrain fracture, i.e., fracture along the grain boundaries, has taken place.Samples with larger grain sizes tend to exhibit fracture at smaller strains than do samples with smaller grains. Siegel and Fougere observed fracture during tensile testing experiments of nano-crystalline Pd. Recently, Haque and Saif found almost brittle fracture in thin nano-crystalline Al films (30 to 50 nm) with grain sizes varying from 10 to 20 nm. To make sure that the fracture process is not an artifact due to a short annealing time, we doubled the relaxation time and we also relaxed the system at a pressure of 4 GPa with a subsequent relaxation at zero pressure. We did not find any dependence on the aforementioned relaxation procedures. Before the onset of fracture, the plasticity we observed consisted of grain boundary sliding processes and grain growth. For comparison, we did some runs with an EAM Cu potential, revealing no fracture even at large strains. So why does Al show fracture? One explanation is connected to the effective pair potential of the Al interaction used here.The effective pair potential has a double-minima structure that agrees with pseudopotential calculations by Hafner and with other descriptions of Al. As can be seen from the construction of this EAM Al potential, the double-minima structure comes from the relatively low C44 elastic constant of Al. This affects the attractive region of the potential. Holian and Ravelo have shown that changes in the attractive part of the pair potential can enhance brittle fracture over ductile fracture and vice versa. There might be other factors influencing the intergranular fracture process, including the high strain rates used in the simulations. We found an inverse Hall–Petch relation for small grain sizes (Figure 5), i.e., softening with decreasing grain size. The flow stress as a function of 1/d for

nano-crystalline Al shows a linear behavior (the standard error for the regression slope is 0.1 GPa nm). This means that the deformation mechanism for small grain sizes is related to the surface-to-volume ratio of the grains, indicating the dominance of intergrain activity. However, our data points also scale well with d1/2, which is the scaling expected for the Hall–Petch effect (upper inset of Figure 5) (here, the standard error for the regression slope is 0.17 GPa nm1/2).

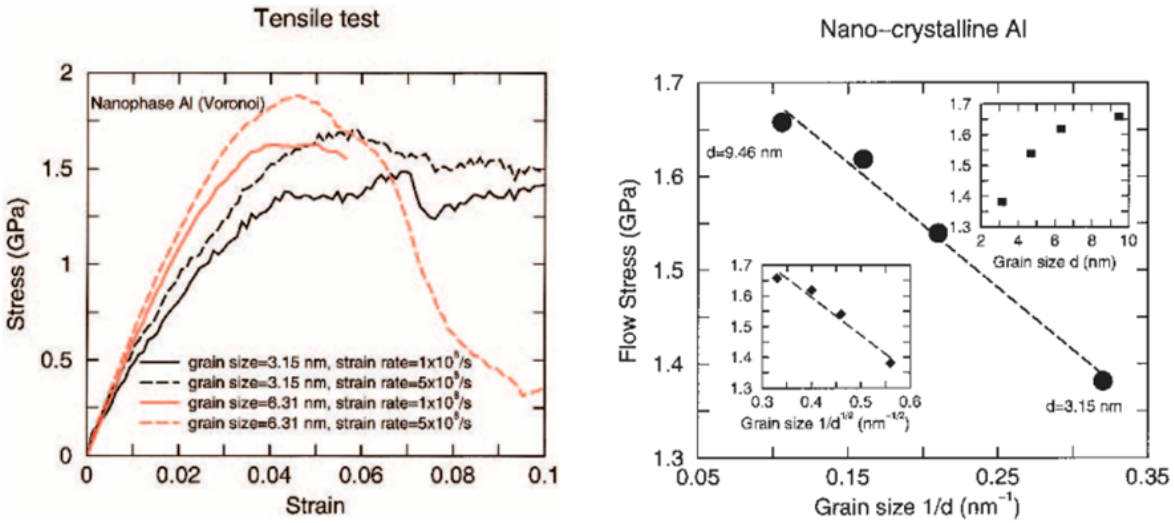

The lower inset of Figure 5 shows the raw data (also shown in Table I) that might suggest that we are close to the turnover into the normal Hall–Petch regime for grain sizes of the order of 10 nm.

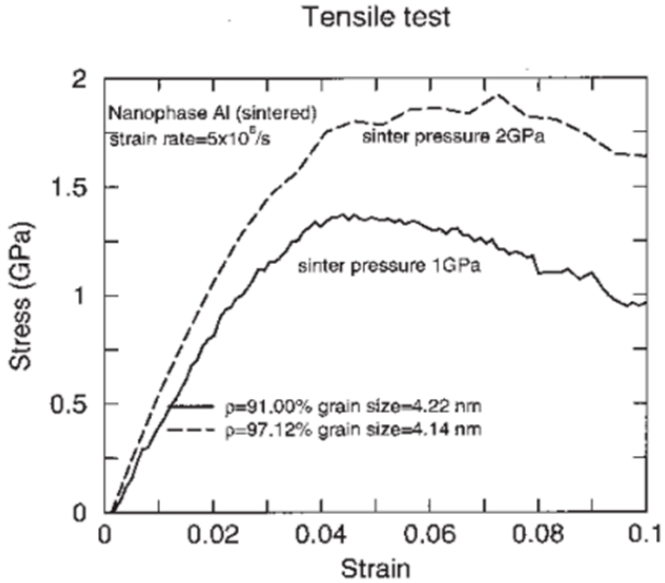

Summary

We have demonstrated an inverse Hall–Petch effect for an EAM model of poly-crystalline Al with grain sizes d 10 nm. At large strains, during the plastic flow process, fracture along the grain boundaries occurs. For sintered samples containing pores, a new mode of plasticity was observed and identified as pore growth. The observed flow stress strongly depends on the sample quality, i.e., higher density or lower porosity. This underlines the importance of the experimental sample quality for investigating mechanical properties in the nanoregime. However, if the samples are sintered under high pressure to a density similar to their Voronoi counterparts, the sintered samples have more mechanical strength. This accounts for the fact that the sintering process leads to better developed grain boundaries as compared to the Voronoi-constructed samples, due to the more free and natural relaxation process. For the largest grain sizes investigated (around 10 nm), the flow stress as a function of grain size gives a hint that the crossover to the Hall–Petch regime is close, which agrees with recent MD simulations of nano-crystalline Cu by Schiøtz and Jacobsen.[25] However, we should emphasize that in order to make a definitive statement, we have to average over several independent samples to obtain statistically significant data points for the flow stress[6] as a function of grain size. It would also be most interesting if the fully threedimensional simulations we discussed in this article are able to describe twinning phenomena in nano-phase Al, as recently found experimentally for grain sizes in the range of 10 to 35 nm.[26] The MD simulations of a thin slab with grain sizes around 50 nm indeed show twinning in Al as a mode of plasticity.[18] However, these simulations, as well as ours, suggest that for the smallest grain sizes investigated here, sliding processes between the grains dominate the plastic deformation process.The experiment showed us how particles behave differently at nano-level regime.The famous hall petch effect gets reverserd at nano level because of dominance of grain boundary effects at nano-level.

Research Article 5

Molecular dynamics analysis of temperature effects on nanoindentation measurement

-Sejal Kotian

Citation
Te-Hua Fang, Cheng-I Weng, Jee-Gong Chang,
Molecular dynamics analysis of temperature effects on nanoindentation measurement,
Materials Science and Engineering: A,
https://doi.org/10.1016/S0921-5093(03)00219-3

Abstract:

A three-dimensional molecular dynamics (MD) model is carried out to study the effects of temperature on the atomic-scale nanoindentation process. The model utilizes the **Morse potential function** to simulate interatomic forces between the sample and tool. The results show that both Young's modulus and hardness become smaller as temperature increases. The results also indicate that elastic recovery is smaller at higher temperatures. In addition, some defects of vacancies, atomic steps, and plastic indent are observed on the surface region.

Introduction:
MD simulation of nanoindentation has been used to investigate various aspects of the interaction between the **tool tip and the workpiece.** These have included the phenomena of adhesion
and fracture of the workpiece, nanoscale etching and indentation by a carbon nanotube, phase transformations, elastic and plastic contact behavior, and the influence of different tool materials on the indention mechanism

The most popular method for determining thin film characteristics like Young's modulus and hardness is **nanoindentation**. However, extensive redesign and development of nanoindentation measurement methods, with a focus on tips, are required to provide accurate measurements of film properties, particularly for very thin films of the order of 1 nm. The controlled and reliable small-depth penetration needed to reduce substrate impacts during thin film measurements is challenging to maintain with current techniques. Moreover, the influence of environmental conditions such as temperature and moisture can have significant effects on system performance. On the other hand,

these difficulties with traditional experimental methodology can, in general, be easily solved by the use of molecular dynamics (MD) simulation

It is common knowledge that temperature has a substantial impact on tribological qualities. Furthermore, when an object gets smaller and smaller, the effects of temperature grow more significant. This study's major goal is to use MD simulation to assess how temperature affects the tribological characteristics of nanoindentation. The interatomic forces between atoms are modeled using the Morse potential. The workpiece's hardness and Young's modulus are calculated using the load/distance depth curves produced by the indentation simulation.

Simulation Model:

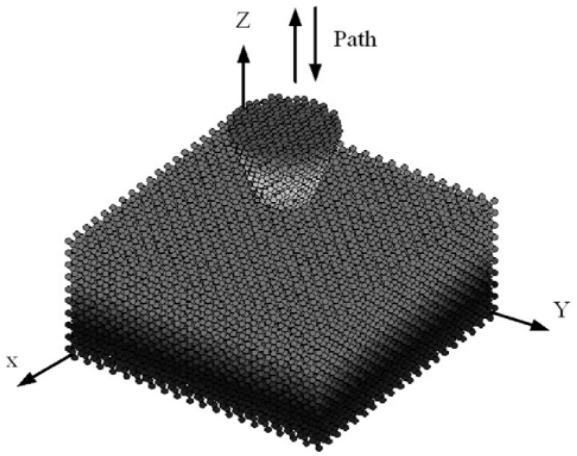

Fig. 1. MD simulation model.

A sample workpiece and a tool are assumed to consist, respectively, of monocrystalline copper and rigid diamond, as shown above.
Periodic boundary conditions are used in the transverse (x and y) directions, and the bottom three layers of atoms of copper are fixed in space. The force acting on an individual atom is obtained by summing the forces contributed by the surrounding atoms. The Morse potential is written as:

$$\text{Morse potential:}$$
$$V(r) = D_e\left([1 - e^{-a(r-r_e)}]^2 - 1\right)$$

where V(r) is a pair potential energy function, the cohesive energy D, the equilibrium distance r0, and the elastic parameter a, are usually fitted to the bulk modulus.
The force on atom i resulting from the interaction of all the other atoms can be derived from the above potential function,

As the data (tool velocity, integration time, etc.) are input, the initial displacement of the sample material is created from a face-centered cubic (FCC) copper lattice. Initial velocities are assigned from the Maxwell distribution, and the magnitudes are adjusted so as to keep the temperature in the system constant according to the below equation

$$v_i^{\text{new}} = \left\{ \frac{N_f N k_B T_0}{2} \left[\sum_{i=1}^{N} \frac{m_i (v_i^{\text{old}})^2}{2} \right]^{-1} \right\}^{1/2} v_i^{\text{old}}$$

The initial displacement and velocity are values determined independently, and the time integration of motion is performed by Gear's fifth predictor/corrector method.

Results:

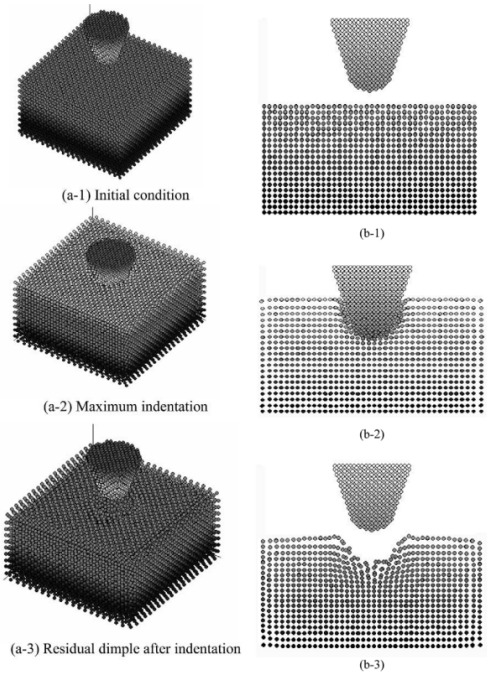

Fig. 3. (a) Positions at different stages of the nanoindention process. (b) Positions at different stages of the nanoindention process.

A residual dimple in the copper is observed after indentation by the diamond tool, as shown in Fig. 3(a-3). The formation of this residual dimple is due to unrecoverable plastic deformation. At maximum indentation depth (Fig. 3(a-3) and (b-3)), it is observed that the atomic order beneath the indenter differs considerably from its original pattern.

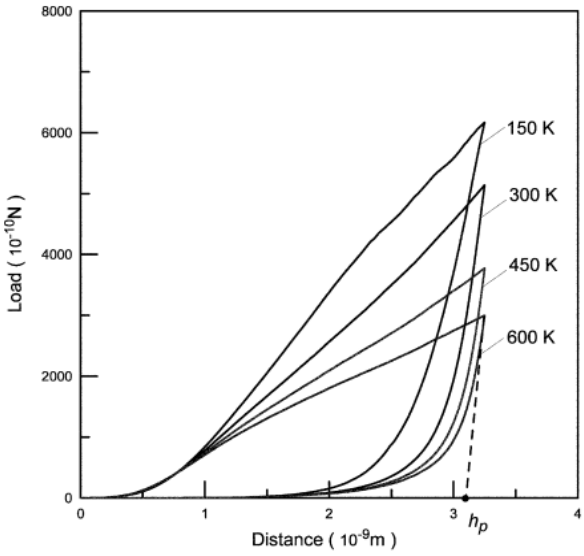

Fig. 4. Load–distances of nanoindentation process varies at different temperatures.

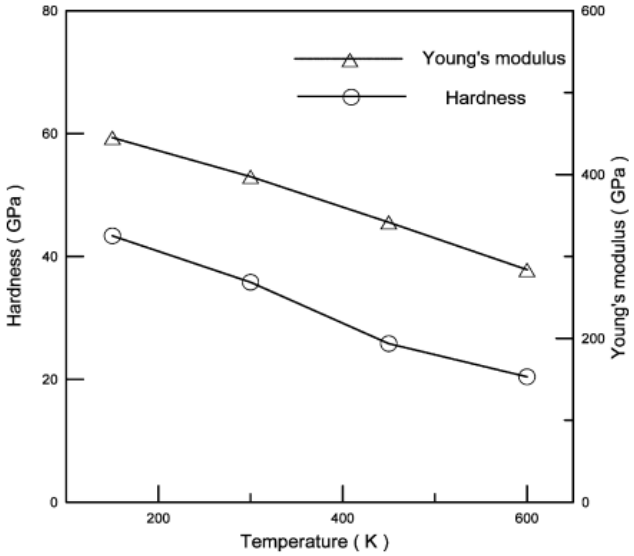

Fig. 6. Young's modulus and hardness at different temperatures.

Load/distance curves for nanoindentations on copper with various temperature conditions are shown in Fig. 4. As the indentation depth of the rigid tip continues to increase, the load curve starts to go up until it reaches a maximum depth. After reaching the maximum depth, the tip begins to unload and return to its original position. Using the intersection of the tangential line of the unloading curve at the x-axis to define the plastic indentation depth, hp(=hmax-Wmax/Smax), the plastic indentation depth is seen to increase with increasing temperature. This also means that elastic recovery is smaller at a higher temperatures. The explanation of this phenomenon from the microscopic viewpoint is that the workpiece interatomic interaction forces, including repulsive and attractive forces, become weaker as the workpiece interatomic distance increases as a result of higher temperature.

Conclusion:

Temperature effect on the tribological properties:

According to Fig. 4, which depicts the relationship between load and indentation depth, Young's modulus and hardness are assessed from the indentation curve.

Figure 6 depicts the connection between copper's mechanical characteristics and temperature. The MD indentation curve depicted in Fig. 4 is used to calculate these properties. As the temperature rises, Young's modulus and hardness both decline. This behaviour is consistent with the macro-behaviour.From a micro-scale perspective, the interatomic bonding energy of the workpiece reduces as interatomic distance and temperature rise, which results in a reduction in hardness

REFERENCES

1. R.W. Siegel: Physics of New Materials, Updated ed., Springer-Verlag, Heidelberg, 1998, pp. 66-106.

2. E.O. Hall: Proc. Phys. Soc. London, 1951, vol. 64, pp. 747-53.

3. N.J. Petch: J. Iron Steel Inst., 1953, vol. 174, pp. 25-28.

4. A.H. Chokshi, A. Rosen, J. Karch, and H. Gleiter: Scripta Metall. Mater., 1989, vol. 23, pp. 1679-84.

5. T.G. Nieh and J. Wadsworth: Scripta Metall. Mater., vol. 25, pp. 955-58.

6. J. Schiøtz, F.D. Di Tolla, and K.W. Jacobsen: Nature (London), 1998, vol. 391, pp. 561-63.

7. C.C Koch and J. Narayan: Mat. Res. Soc. Symp. Proc., 2001, vol. 634, pp. B5.1.1-B5.1.11.

8. J. Schiøtz, T. Vegge, F.D. Di Tolla, and K.W. Jacobsen: Phys. Rev. B, 1999, vol. 60, pp. 11971-11983.

9. H. Van Swygenhoven and A. Caro: Appl. Phys. Lett. B, 1997, vol. 71, pp. 1652-54.

10. M.P. Allen and D.J. Tildesley: Computer Simulation of Liquids, Clarendon Press, Oxford, United Kingdom, 1987; D.C. Rapaport: The Art of Molecular Dynamics Simulation, Cambridge University Press, Cambridge, United Kingdom, 1995; W.G. Hoover: Time Reversibility, Computer Simulation, and Chaos, World Scientific, Singapore, 1999.

11. The SPaSM (“Scalable Parallel Short-Range Molecular Dynamics”) code is described in P.S. Lomdahl, P. Tamayo, N. Grønbech-Jensen,

and D.M. Beazley: Proc. Supercomputing 93, G.S. Ansell, ed., IEEE

Computer Society Press, Los Alamitos, CA, 1993, pp. 520-27; D.M.

Beazley and P. 12. M.S. Daw and M.I. Baskes: Phys. Rev. Lett., 1983, vol. 50, pp. 1285-88.

13. S. Grabowski, K. Kadau, and P. Entel: Phase Transitions, 2002, vol. 75,

pp. 265-72.

14. E.A. Stern, R.W. Siegel, M. Newville, P.G. Sanders, and D. Haskel:

Phys. Rev. Lett., 1995, vol. 75, pp. 3874-77.

15. H. Van Swygenhoven, D. Farkas, and H. Caro: Phys. Rev. B, 2000,

vol. 62, pp. 831-38.

16. M. Jean: Methods Appl. Mech. Engg., 1999, vol. 177, pp. 235-57.

17. D. Kadau, G. Bartels, L. Brendel, and D.E. Wolf: Computer Physics

Communications, 2002, vol. 147, pp. 190-93.

18. V. Yamakov, D. Wolf, S.R. Phillpot, A.K. Mukherjee, and H. Gleiter:

Nature Mater., 2002, vol. 1, pp. 1-4.

19. R.W. Siegel and G.E. Fougere: NanoStr. Mater., 1995, vol. 6,

pp. 205-16.

20. M.A. Haque and M.T. A Saif: Scripta Mater., 2002, vol. 47, pp. 863-67.

21. Movies of the simulations are available at http://www.thp.uni-duisburg.

de/kai/index_1.html/

22. A.F. Voter: Phys. Rev. B, 1998, vol. 57, pp. 13985-13988.

23. J. Hafner: Electron Theory in Alloy Design, The Institute of Materials,

London, 1992.

24. B.L. Holian and R. Ravelo: Phys. Rev. B, 1995 vol. 51, pp. 11275-11288.

25. J. Schiøtz and K.W. Jacobsen: Sci., 2003, vol. 301, pp. 1357-59.

26. M. Chen, En Ma, K.J. Hemker, H. Sheng, and Y. Wang, and X. Cheng:

Science, 2003, vol. 300, pp. 1275-77.

S. Lomdahl: Computers in Physics, 1997